Article

Solution-Processed Anodes from Layer-Structure Materials for High-Efficiency Polymer Light-Emitting Diodes

Gitti L. Frey, Kieran J. Reynolds, Richard H. Friend, Hagai Cohen, and Yishay Feldman

J. Am. Chem. Soc., **2003**, 125 (19), 5998-6007• DOI: 10.1021/ja020913o • Publication Date (Web): 16 April 2003

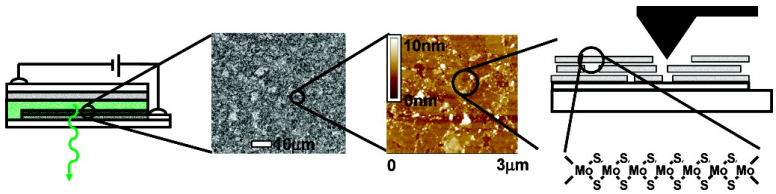

More About This Article

Additional resources and features associated with this article are available within the HTML version:

- Supporting Information
- Links to the 5 articles that cite this article, as of the time of this article download
- Access to high resolution figures
- Links to articles and content related to this article
- Copyright permission to reproduce figures and/or text from this article

View the Full Text HTML

J|A|C|S
ARTICLES
Published on Web 04/16/2003

Solution-Processed Anodes from Layer-Structure Materials for High-Efficiency Polymer Light-Emitting Diodes

Gitti L. Frey,*,† Kieran J. Reynolds,† Richard H. Friend,† Hagai Cohen,‡ and Yishay Feldman‡

Contribution from the Cavendish Laboratory, Department of Physics, University of Cambridge, Madingley Road, Cambridge CB3 0HE, U.K., and Surface Analysis Lab, Chemical Services Unit, Weizmann Institute of Science, Rehovot 76100 Israel

Received July 3, 2002; E-mail: gitti@technion.ac.il

Abstract: The development of low-cost, large-area electronic applications requires the deposition of active materials in simple and inexpensive techniques at room temperature, properties usually associated with polymer films. In this study, we demonstrate the integration of solution-processed inorganic films in light-emitting diodes. The layered transition metal dichalcogenide (LTMDC) films are deposited through Li intercalation and exfoliation in aqueous solution and partially oxidized in an oxygen plasma generator. The chemical composition and thickness of the LTMDC and corresponding transition metal oxide (TMO) films are investigated by X-ray photoelectron spectroscopy. The morphology and topography of the films are studied by atomic force microscopy. X-ray powder diffraction is used to determine the orientation of the LTMDC film. Finally, the LTMDC and their corresponding oxides are utilized as hole-injecting and electron-blocking materials in polymer light-emitting diodes with the general structure ITO/LTMDC/TMO/polyfluorene/Ca/Al. Efficient hole injection and electron blocking by the inorganic layers result in outstanding device performance and high efficiency.

Introduction

The successful integration of semiconducting polymers into electronic devices such as light-emitting diodes[1,2] and field-effect transistors[3,4] has generated a wide academic and industrial interest in these materials and device structures. A main advantage of electronic devices based on polymers is the room-temperature solution processing of the polymers into thin films, which leads to easy and low-cost fabrication of the devices. The deposition of polymer films is fairly simple and is usually done through spin-coating, dip-coating, layer-by-layer deposition, or self-assembly techniques. Nevertheless, electronic devices based on inorganic materials still dominate the market due to their well-defined and wide spectrum of electronic properties. However, the deposition of thin inorganic films presently involves the use of difficult and expensive fabrication techniques, such as high-vacuum evaporation. Hence, solution processing of inorganic materials into thin films and their integration as functional layers in electronic devices is desirable. Recently, Kagan et al.[5] reported the integration of hybrid inorganic−organic materials as the active layer in field-effect transistors. These hybrid perovskites, some of which are solution-processable, naturally form layered structures with alternating inorganic and organic sheets.[6−9]

Another family of inorganic layered materials, the layered transition metal dichalcogenides (LTMDC), displays a wide range of the electronic properties suitable for a variety of electronic devices. Furthermore, the layered structure of these materials enables them to be chemically processed into ultrathin films via intercalation and exfoliation.

The structure of the layered transition metal dichalcogenides, MX_2 (M = Ti, Zr, Hf, V, Nb, Ta, Mo, W, etc. and X = S, Se, Te) is derived from hexagonal sheets of metal atoms sandwiched between two hexagonal sheets of chalcogen atoms. The X−M−X sheets are covalently bonded, while adjacent MX_2 layers interact via van der Waals forces.[10] The weak bonding between layers leads to highly anisotropic mechanical and electrical properties. Furthermore, the surface of these materials has no dangling bonds and, hence, is chemically inert. The coordination and the oxidation state of the metal atom determine the electronic properties of the material. For example, group V metal atoms (Nb, Ta) are in a trigonal prismatic coordination and the corresponding dichalcogenide materials are metals. Group VI atoms (Mo, W) are also in a trigonal prismatic coordination but have a full d_{Z^2} band, and hence, the corre-

† University of Cambridge.
‡ Weizmann Institute of Science.

(1) Burroughes, J. H.; Bradley, D. D. C.; Brown, A. R.; Marks, R. N.; Mackay, K.; Friend, R. H.; Burns, P. L.; Holmes, A. B. *Nature* **1990**, *347*, 539.
(2) Friend, R. H.; Gymer, R. W.; Holmes, A. B.; Burroughes, J. H.; Marks, R. N.; Taliani, C.; Bradley, D. D. C.; Dos Santos, D. A.; Bredas, J. L.; Logdlund, M.; Salaneck, W. R. *Nature* **1999**, *397*, 121.
(3) Bao, Z.; Dodabalapur, A.; Lovinger, A. J. *Appl. Phys. Lett.* **1996**, *69*, 4108.
(4) Sirringhaus, H.; Tessler, N.; Friend, R. H. *Science* **1998**, *280*, 1741.
(5) Kagan, C. R.; Mitzi, D. B.; Dimitrakopoulos, C. D. *Science* **1999**, *286*, 945.
(6) Mitzi, D. B. *Chem. Mater.* **2001**, *13*, 3283.
(7) Mitzi, D. B.; Dimitrakopoulos, C. D.; Kosbar, L. L. *Chem. Mater.* **2001**, *13*, 3728.
(8) Mitzi, D. B.; Chondroudis, K.; Kagan, C. R. *Inorg. Chem.* **1999**, *38*, 6246.
(9) Chondroudis, K.; Mitzi, D. B. *Appl. Phys. Lett.* **2000**, *76*, 58.
(10) Wilson, J. A.; Yoffe, A. D. *Adv. Phys.* **1969**, *18*, 193.

10.1021/ja020913o CCC: $25.00

sponding dichalcogenide materials are semiconductors (2H-MX_2). MoS_2 and WS_2 can also have octahedral coordination, in which case they are metallic (1T-MS_2).[11] The work function values of various layered metal dichalgogenides have been measured by photoemission and are in the range of 4.2−5.9 eV.[10,12,13]

Thin films of the LTMDC have been prepared through Li intercalation and exfoliation in water.[11,14,15] In the intercalated compounds, the Li atoms are situated in the van der Waals gap. Addition of water to the intercalated material results in the reduction of the water by the intercalated Li. The intercalation and reduction reactions are shown below:

$$\text{YBu-Li} + MX_2 \rightarrow \text{Li}_y MX_2 + (Y/2)C_8H_{18}$$

$$\text{Li}_y MX_2 + YH_2O \rightarrow \text{YLiOH} + (Y/2)H_2 + MX_2$$

The H_2 gas evolving between the MX_2 layers breaks up the stacking of the layers. As a result of the exfoliation process, a suspension of single layers (SL) of LTMDC in water is formed. Upon addition of a water-immiscible solvent to the SL aqueous suspension, and agitation of the mixture, a thin film of MX_2 is formed at the solvent/water interface. In a process developed by Morrison, Frindt, and Divigalpitiya[16,17] the film is transferred onto a wet hydrophilic substrate by dipping the lower end of the substrate into the solvent/water interface.

Recently, we reported the fabrication of high-efficiency polymer electroluminescent devices (PLEDs) comprising LTMDC thin films.[18] In these devices, the LTMDC and their corresponding oxides are utilized as hole-injecting and electron-blocking materials in the device situated between an ITO anode and the polymer emissive layer.

The fundamental process in organic electroluminescent devices involves the injection of holes and electrons from the electrodes into the emissive material to form neutral bound excited states (excitons) that can relax through photon emission. Initially, the structure of PLEDs involved a thin film of the emitting polymer sandwiched between a transparent hole-injecting electrode (anode) and an electron-injecting electrode (cathode).[1] The progress in understanding the processes controlling the device properties has led to a multilayer device structure comprising one or more active layers such as the following: injecting, transporting or blocking layers, in addition to the emitting layer, sandwiched between the electrodes.[2] These active layers enhance charge injection and transport in the device and balance the hole and electron currents, resulting in high-performance devices.

Efficient injection of holes into the HOMO level of a light-emitting polymer requires a hole-injecting material with a work function value (Φ) higher than the ionization potential (Ip) of the polymer. In polyfluorenes, a widely used family of high-efficiency photoluminescent semiconducting polymers, the Ip is in the range of 5.3−5.9 eV.[19,20] ITO is commonly used as the anode in PLEDs due to its semitransparency in the visible region and its fairly high work function, $\Phi = 4.7$ eV.[21] However, the 1-eV barrier at the ITO/polyfluorene interface prevents efficient hole injection into the device. For improved hole injection, a thin film of poly-(3,4-ethylene dioxythiophene−poly(styrenesulfonate) (PEDOT−PSS) is commonly spun on the ITO anode.[22] The work function of PEDOT, $\Phi = 5.1$ eV, reduces the barrier to hole injection. Recently, it was shown that a phase segregation occurs in the PEDOT−PSS system resulting in a predominance of PSS in the surface region.[23] It was suggested that the insulating PSS acts as an electron-blocking material and forms a barrier for electron extraction.[24] In this model, the offset between the energy levels of PSS and the emitting polymer builds a potential barrier at the polymer/polymer interface. The blocking layer (PSS) immobilizes the electrons and confines them to the blocking layer/emissive layer interface. The high electron density at this interface ensures that the holes pass within a collision capture radius of an electron.

Enhancing hole injection into polyfluorenes is possible through deposition of materials with work function values higher than those of ITO and PEDOT. The LTMDC layered compounds are promising materials as hole injectors due to their high work functions. The transition metal oxides (TMOs), on the other hand, are wide-gap semiconductors and can be utilized as an electron-blocking layer. In this paper, we report in detail the preparation, characterization, and integration of solution-processed ultrathin MoS_2/MoO_3 and $NbSe_2/Nb_2O_5$ films as hole-injecting/electron-blocking layers in PLEDs. The efficient hole-injecting and electron-blocking by the inorganic layers improves carrier balancing in the device and leads to significant enhancements in device performance and efficiency. Furthermore, the combination of the LTMDC and TMO electronic and chemical properties offers the ability to tailor and control the device properties.

Experimental Section

Film Deposition. Li_xMoS_2 and Li_xNbSe_2 were prepared by addition of BuLi (1.6 M in hexanes, Aldrich) to 2H-MoS_2 powder (Aldrich) and $NbSe_2$ powder (Alfa Aesar) under argon, following the procedure given in refs 14 and 15. A total of 10−15 mg of the Li intercalated solid was exfoliated in 7−10 mL of water (Millipore, 18 MΩ/cm) in an ultrasonic bath for 60 min. The suspension was centrifuged, and the sediment was redispersed in water. This process was repeated until the pH of the suspension reached 7, (usually three or four times). Upon addition of *p*-xylene (Aldrich) to the water suspension, and agitation of the mixture, a thin film of MX_2 is formed on the xylene/water interface. The film is transferred onto a wet substrate by dipping the lower end of the substrate into the solvent/water interface. The exfoliation and film forming were performed following the procedure given in refs 16 and 17. $NbSe_2$ films for absorption and X-ray diffraction (XRD) measurements and MoS_2 films were annealed in vacuum

(11) Acrivos, J. V.; Liang, W. Y.; Wilson, J. A.; Yoffe, A. D. *J. Phys. C* **1971**, *4*, L18.
(12) Shimada, T.; Ohuchi, F. S.; Parkinson, B. A. *Jpn. J. Appl. Phys. Part 1***1994**, *33*, 2696.
(13) McMenamin, J. C.; Spicer, W. E. *Phys. Rev. B* **1977**, *16*, 5474.
(14) Murphy, D. W.; Di Salvo, F. J.; Hull, G. W.; Waszczak, V. *Inorg. Chem.* **1976**, *15*, 17.
(15) Joensen, P.; Frindt, R. F.; Morrison, S. R. *Mater. Res. Bull.* **1986**, *21*, 457.
(16) Divigalpitiya, W. M. R.; Frindt, R. F.; Morrison, S. R. *Science* **1989**, *246*, 369.
(17) Divigalpitiya, W. M. R.; Morrison, S. R.; Frindt, R. F. *Thin Solid Films* **1990**, *186*, 177.
(18) Frey, G. L.; Reynolds, K. J.; Friend, R. H. *Adv. Mater.* **2002**, *14*, 265.
(19) Bernius, M. T.; Inbasekaran, M.; O'Brien, J.; Wu, W. S. *Adv. Mater.* **2000**, *12*, 1737.
(20) Campbell, A. J.; Bradley, D. D. C.; Antoniadis, H. *J. Appl. Phys.* **2001**, *89*, 3343.
(21) Kim, J. S.; Granstrom, M.; Friend, R. H.; Johansson, N.; Salaneck, W. R.; Daik, R.; Feast, W. J.; Cacialli, F. *J. Appl. Phys.* **1998**, *84*, 6859.
(22) Groenendaal, B. L.; Jonas, F.; Freitag, D.; Pielartzik, H.; Reynolds, J. R. *Adv. Mater.* **2000**, *12*, 481.
(23) Greczynski, G.; Kugler, T.; Keil, M.; Osikowicz, W.; Fahlman, M.; Salaneck, W. R. *J. Electron Spectrosc. Relat. Phenom.* **2001**, *121*, 1.
(24) Murata, K.; Cina, S.; Greenham, N. *Appl. Phys. Lett.* **2001**, *79*, 1193.

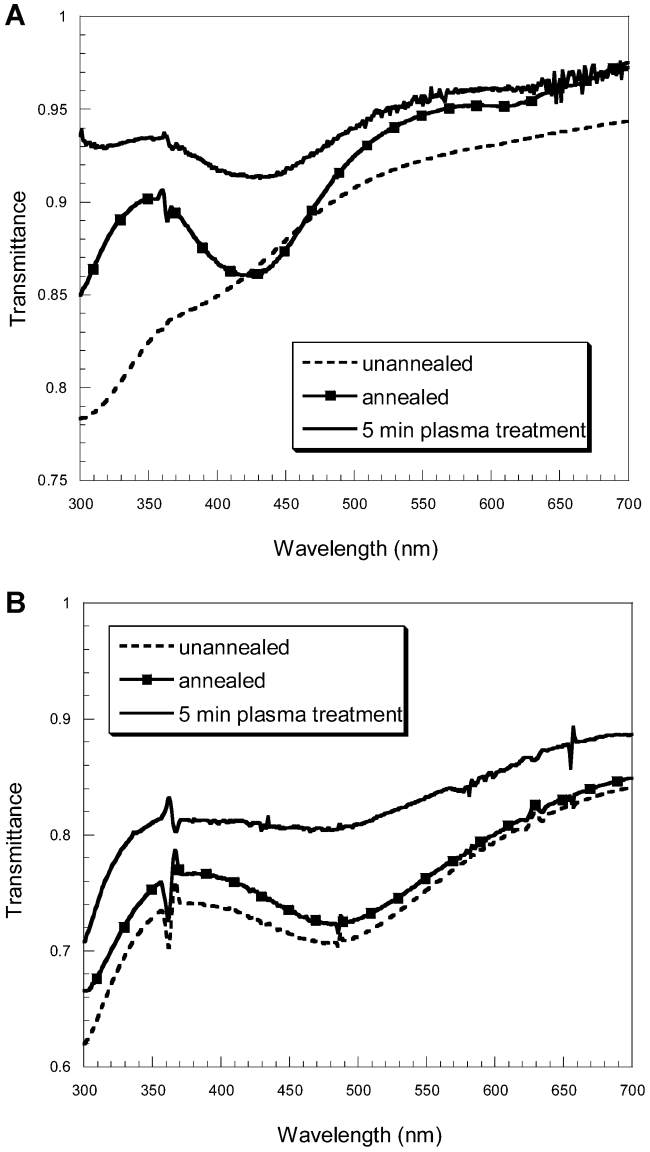

Figure 1. Transmittance spectra of as-deposited, annealed, and oxygen plasma treated (5 min) of (A) MoS_2 films and (B) $NbSe_2$ films.

($\sim 10^{-5}$ mbar) at 220 °C for 10 h, while $NbSe_2$ films for atomic force microscopy (AFM) and devices were not annealed. The MoS_2 and $NbSe_2$ films were then treated in an oxygen plasma generator for 0, 0.1, 1, 5, 10, or 20 min. Pure oxygen was fed to a commercial plasma etcher at a pressure of $\sim$0.3 mbar in a $<10^{-1}$ mbar vacuum at room temperature. The applied forward and reflected powers were $\sim$250 W and less than 5 W, respectively.

Film Characterization. Transmittance was recorded on a Hewlett-Packard 8453 spectrophotometer. X-ray diffraction (XRD) measurements were performed on a CPS-120 powder diffractometer assembled by spectrolab using Inel hardware and software and a Cu Kα X-ray source. Tapping mode atomic force microscopy (AFM) was performed using a NanoScope IIIa Dimension 3100 (Digital Instruments Inc, Santa Barbara, CA). SEM measurements were performed on a LEO 1530 field emission model, with operating chamber pressure 1×10^{-6} mBar. The sample was biased to 2 kVand $\times$2280 magnification.

X-ray photoelectron spectroscopy (XPS) measurements were carried out with an AXIS-HS Kratos setup, using a monochromatized Al Kα X-ray source ($h\nu = 1486.6$ eV) and pass energies ranging from 20 to 80 eV. The energy scale was calibrated, referring to the C 1s line at $E_B = 284.8$ eV.[25] Differential surface charging was found to be sufficiently small to have a minor effect only on the chemical analysis

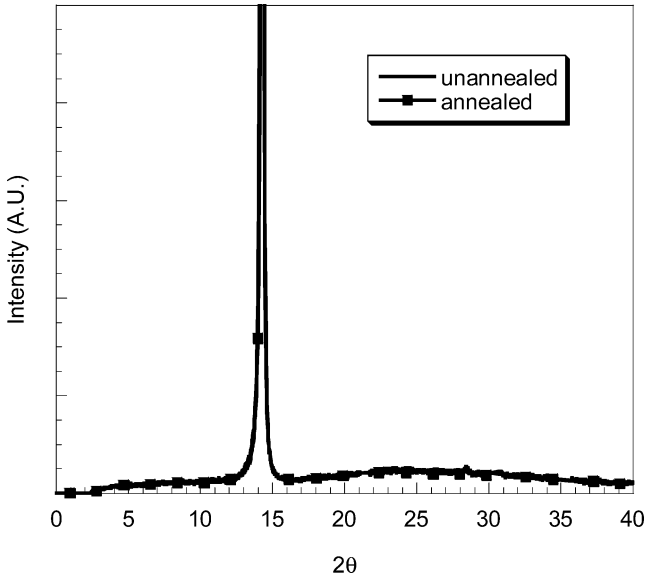

Figure 2. XRD spectra of as-deposited and annealed $NbSe_2$ films.

below. Curve fitting was applied, using Gaussian−Lorenzian line shapes and a Shirley[26] background subtraction.

Angle-resolved XPS (ARXPS)[27] was used for nondestructive depth profiling, taken at a normal (90°) takeoff angle (with respect to the surface plane), as well as at 40° and 30°. These measurements, based on electron attenuation considerations, allow a rough estimate of the surface coverage as well (see text below).

Argon ion sputtering, which is a destructive depth profiling technique, was complementarily applied, using a beam energy of 4 keV and 20 mA emission current, at an incident ion beam angle of 45°. A large-area raster, 4×4 mm^2, was used to verify uniformity across the analysis area. Samples were sputtered at a rate of 3 nm/min, as calibrated on a Ta_2O_5/Ta reference. A first, very short (<1 nm equivalent) sputtering step was taken, removing various ambient surface contaminants (primarily physisorbed O and C), with minimal induced damage. Subsequently, longer sputtering steps gradually revealed the entire overlayer composition.

Samples were transferred to the XPS analysis chamber in medium-quality argon atmosphere.

Device Fabrication and Testing. The 80−100-nm-thick light-emitting polymer films were deposited by spinning a solution of 15 mg/mL polymer in *p*-xylene onto the LTMDC and plasma-treated LTMDC films. Fabrication of 3.1-mm^2 pixels (eight per device) was subsequently completed in a N_2 glovebox without exposure to air. Calcium/aluminum electrodes (100 nm/100 nm) were evaporated through a shadow mask at a base pressure of $<10^{-6}$ mbar. Current density−voltage−luminance (JVL) characteristics were collected under vacuum (10^{-1} mbar) using a Keithley 230 voltage source together with a Keithley 195 digital multimeter; the luminescence output was simultaneously measured using a calibrated Si photodiode collecting 0.1 sr in the forward direction.

Results and Discussion

Transmittance. The transmittance spectra of as-deposited (restacked) and annealed MoS_2 films, 3−7 nm thick, are presented in Figure 1A. The thickness of the LTMDC films is controlled through the concentration of the exfoliated suspen-

(25) *Handbook of X-ray Photoelectron Spectroscopy*; Chastain, J., Ed.; Perkin-Elmer: Eden Prairie, MN, 1992.
(26) Shirley, D. A. *Phys. Rev. B* **1972**, *5*, 4709.
(27) *Practical Surface Analysis*; Briggs, D., Seeah, M. P., Eds.; Wiley: Chichester, U.K., 1984; p 164.

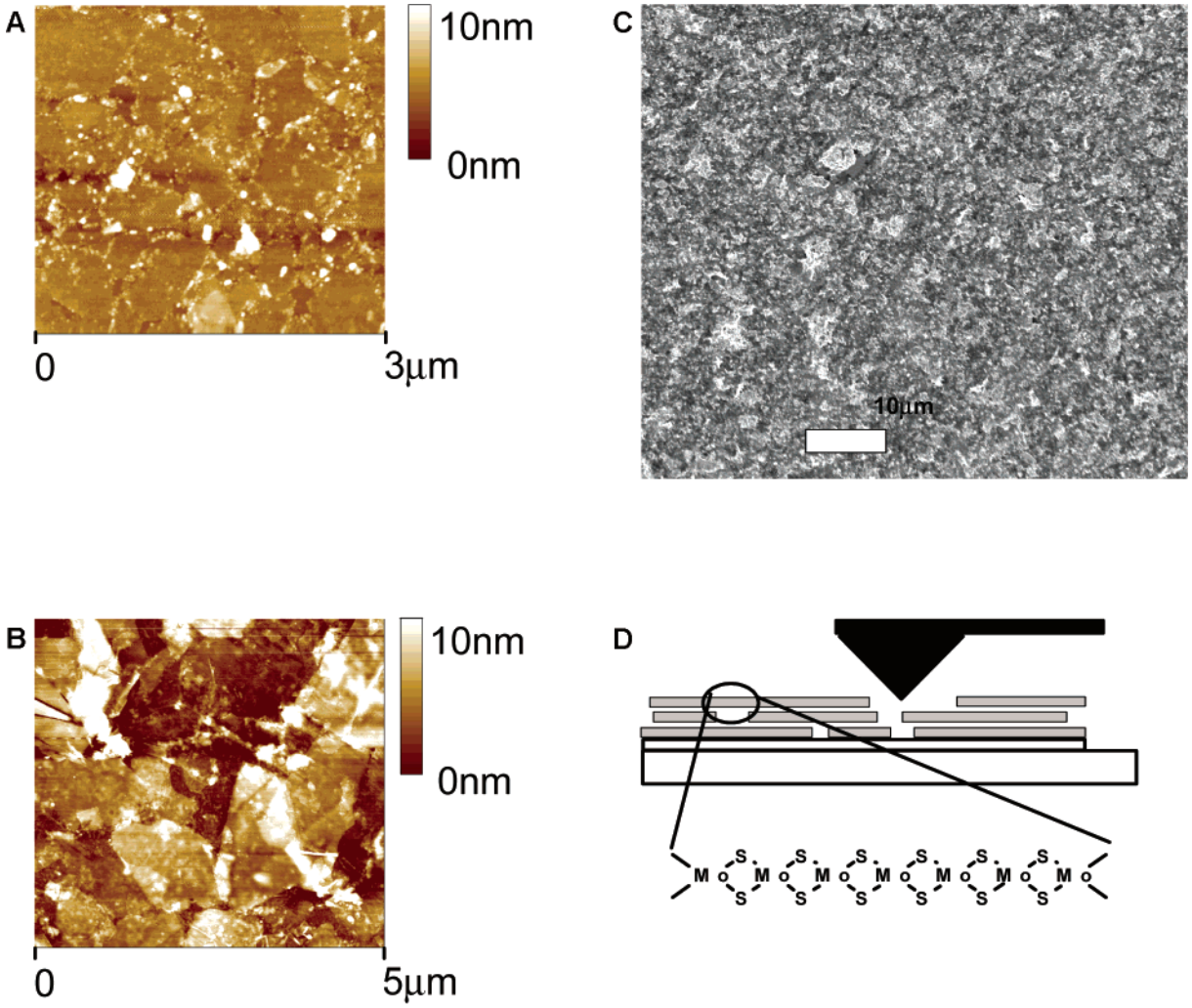

Figure 3. (A) AFM micrograph of an MoS_2 film, (B) AFM micrograph of an $NbSe_2$ film, (C) SEM micrograph of an MoS_2 film, and (D) schematic diagram of an MX_2 film.

Table 1. Transmittance at 550 nm as a Function of Plasma Treatment Time

material	plasma etching time (min)	transmittance (%) before plasma treatment	transmittance (%) after plasma treatment	Δ transmittance (%)
MoS_2	0	87	87	0
MoS_2	0.1	86	90	4
MoS_2	1	84	90	6
MoS_2	5	86	94	8
MoS_2	10	84	94	10
MoS_2	20	84	97	13
$NbSe_2$	0	63	63	0
$NbSe_2$	0.1	72	75	3
$NbSe_2$	1	77	83	6
$NbSe_2$	5	65	73	8
$NbSe_2$	10	67	77	10
$NbSe_2$	20	75	86	11

sion, and the transmittance at 550 nm in all films is over 85% (see Table 1).

Li intercalation of 2H-MoS_2 results in a structural transformation within the layers, causing the geometry around the metal atoms to shift from trigonal prismatic to octahedral.[23] The intercalated Li atom donates a partial negative charge to the MoS_2 system, which is stabilized by a reorganization of the Mo atom coordination. The trigonal prismatic-to-octahedral shift is accompanied by a semiconductor to metallic transition.[28,29] The octahedral structure and metallic properties are preserved in the exfoliated material and restacked films.[30−32]

The broad featureless transmittance spectrum of as-deposited MoS_2 indicates a metallic MoS_2 phase.[15] However, the octahedral phase is metastable and reverts to the semiconducting phase through annealing.[33,34] Indeed, upon annealing, two shoulders and a broad dip at 660, 600, and 430 nm, respectively, are noticeable in the spectrum. These features are in good agreement with the A, B, and C excitons in the absorption spectrum of bulk 2H-MoS_2 semiconducting phase.[10,35]

Figure 1B shows the transmittance spectra of as-deposited (restacked) and annealed $NbSe_2$ films 5−10 nm thick. Both spectra display a dip at 500 nm on top of the broad background, characteristic of bulk $NbSe_2$.[10] $NbSe_2$ does not reorganize with

(28) Py, M. A.; Haering, R. R. *Can. J. Phys.* **1983**, *61*, 76.
(29) Bissessur, R.; Kanatzidis, M. G.; Schindler, J. L.; Kannewurf, C. R. *J. Chem. Soc., Chem. Commun.* **1993**, 1582.
(30) Heising, J.; Kanatzidis, M. G. *J. Am. Chem. Soc.* **1999**, *121*, 11720.
(31) Heising, J.; Kanatzidis, M. G. *J. Am. Chem. Soc.* **1999**, *121*, 638.
(32) Gordon, R. A.; Yang, D.; Crozier, E. D.; Jiang, D. T.; Frindt, R. F. *Phys. Rev. B* **2002**, *65*, 125407.
(33) Wypych, F.; Schollhorn, R. *J. Chem. Soc., Chem. Commun.* **1992**, 1386.
(34) Tsai, H. L.; Heising, J.; Schindler, J. L.; Kannewurf, C. R.; Kanatzidis, M. G. *Chem. Mater.* **1997**, *9*, 879.
(35) Frey, G. L.; Elani, S.; Homyonfer, M.; Feldman, Y.; Tenne, R. *Phys. Rev. B* **1998**, *57*, 6666.

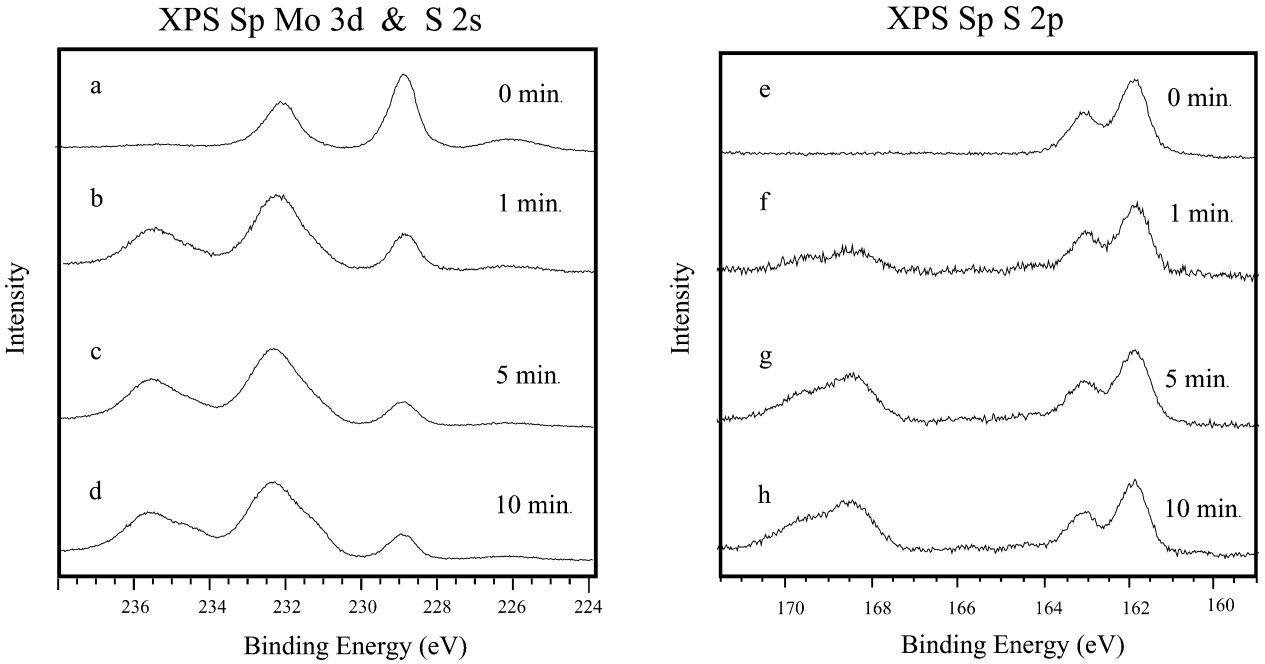

Figure 4. Mo 3d and S 2s XPS lines (a−d) and S 2p XPS line (e−h) of MoS_2 films after 0- (a, e), 1- (b, f), 5- (c, g), and 10-min (d, h) oxidation.

intercalation or exfoliation, and hence, the transmittance spectra in the visible range of the annealed and unannealed $NbSe_2$ films are identical.[11]

The transmittance spectrum of a LTMDC film after 5-min oxygen plasma treatment is also presented in Figure 1. Upon oxygen plasma treatment, the nature of the spectra does not change but the intensity increases, indicating that some of the LTMDC material is consumed. The increase in the transmittance of the films at 550 nm (the photoluminescence peak of the emitting polymer) as a function of plasma treatment time is listed in Table 1. The pronounced increase in transmittance even after a very short plasma treatment indicates that the initial conversion of the LTMDC film is very rapid. However, the conversion rate decreases with time. This rate decrease alludes to an oxidation process in which the outer part of the LTMDC film is rapidly oxidized in the plasma treatment. Oxidizing the inner part of the film is slower since it requires the diffusion of oxygen into the film and of sulfur or selenide species out of the film. This process is later corroborated by XPS.

X-ray Powder Diffraction. The LTMDC films studied by XRD were thicker, ∼30 nm thick, than those used for transmittance, AFM and XPS measurements, and integrated into devices, as these films were too thin to produce readily detectable signals. The as-deposited LTMDC films have only one peak identified in the (00*l*) direction corresponding to *c*-axis spacings of 6.15 (MoS_2) and 6.25 Å ($NbSe_2$). The 6.15-Å spacing in MoS_2 is in good agreement with XRD spectra of MoS_2 single crystals,[10,36] exfoliated−restacked material,[15] and thin films.[17] Upon annealing, the width of the peak in the MoS_2 spectrum decreases while its intensity increases, demonstrating an improvement in the ordering of the layers in the *c*-axis direction, in good agreement with literature reports.[17] $NbSe_2$ exfoliated−restacked thin films were not extensively investigated prior to this study. The 6.25-Å spacing obtained for the as-deposited $NbSe_2$ is in good agreement with the corresponding bulk materials[10,36] and is presented in Figure 2. The $NbSe_2$ diffraction was not affected by annealing. Furthermore, the diffraction of the 30-nm-thick $NbSe_2$ and MoS_2 films did not change after 5-min oxygen plasma treatment (not shown). This indicates that the quantity of any crystalline material formed is insufficient to be detected and that the as-deposited LTMDC material is still present, in the ordered form it was deposited in.

AFM and SEM. The orientation of the LTMDC layers parallel to the substrate leads to the steplike mosaic structure shown by AFM for MoS_2 and $NbSe_2$ in Figure 3A and B, respectively. The platelets are ∼0.5−2 μm long in the MoS_2 films and slightly larger in the $NbSe_2$ films. The steps are <10 nm in both cases, as seen in cross section analysis. The MoS_2 SEM micrograph in Figure 3C shows that the film is continuous over millimeters. The step-structured topography of the film surface is schematically illustrated in Figure 3D.

X-ray Photoelectron Spectroscopy. XPS measurements were performed on thin films of MoS_2 and of $NbSe_2$ and films of both materials subjected to a series of oxygen plasma treatments as described in the Experimental Section. XPS spectra of the metal and chalcogen atoms as a function of plasma treatment in MoS_2 and $NbSe_2$ are presented in Figures 4 and 6, respectively. The XPS data of both MoS_2 and $NbSe_2$ systems show the deposited LTMDC films as well as their gradual oxidation upon plasma treatment. The spectra demonstrate that both the metal and the chalcogenide elements oxidize during the plasma treatment.[37] The degree of oxidation is quantitatively determined by measuring the atomic ratio (oxidized M divided by total M) at a normal takeoff angle as a function of plasma oxidation time. The increasing degree of oxidation is presented in Table 2.

Figure 4a shows the combined Mo 3d and S 2s XPS spectral window, and Figure 4e shows the S 2p line of an as-prepared

(36) Subba Rao, G. V.; Shafer, M. W. In *Intercalated Layered Materials*; Levy, F., Ed.; D. Reidel: Dordrecht, The Netherlands, 1979; Vol. 6.

(37) Brown, N. M. D.; Cui, N. Y.; McKinley, A. *Appl. Surf. Sci*. **1998**, *134*, 11.

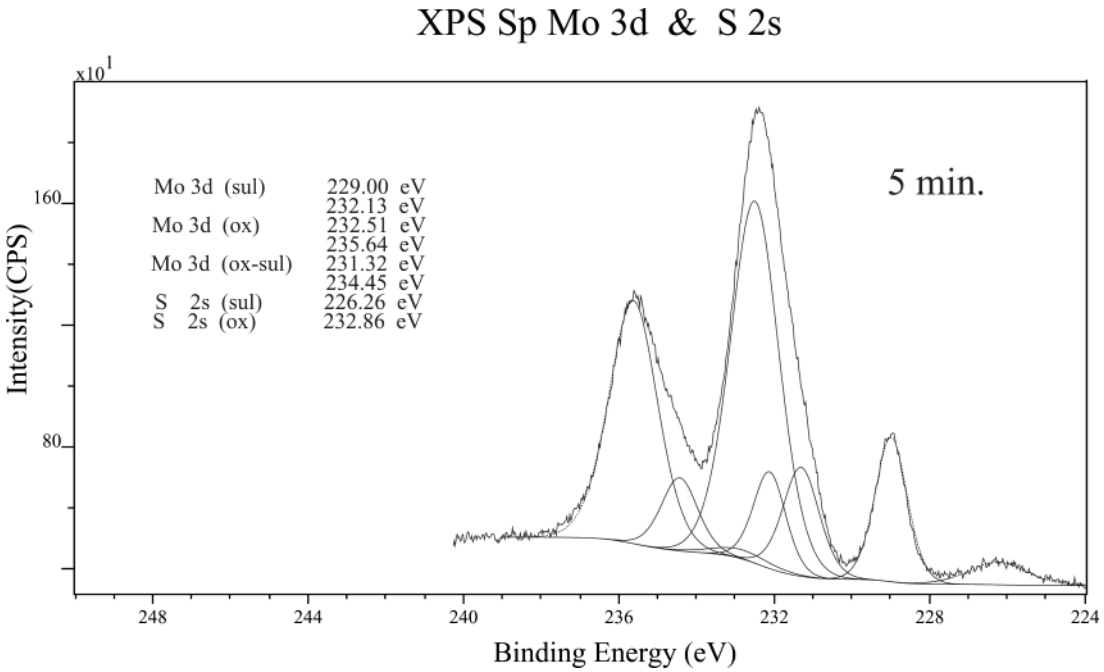

Figure 5. Curve fitting of the Mo 3d and S 2s XPS lines for a 5-min-oxidized MoS_2 film.

Table 2. Binding Energy (eV) and Assignment (Most Likely Compound) of the Characteristic Peaks Found in the XPS Spectra of MoS_2 and $NbSe_2$ as a Function of Oxidation Time[a]

		elements (atom %) and binding energies (eV)										thickness (nm)	
		Mo 3d			S 2p		O 1s	In 3d	Sn 3d	C 1s	deg of oxidn (%)		
material	oxidn time (min)	229 Mo^{sul}	231 Mo^{ox-sul}	232.6 Mo^{ox}	162 S^{2-}	168 S^{ox}	530.6	444.6	486.8	284.8	Mo^{ox}/Mo^{total}	D_1 MoO_3	D_2 MoS_2
MoS_2	0	10.5	0.2	0.4	18.5	0	24.7	9.5	1.9	34.3	5	0.1	2.8
	0.1	3	1.4	5.7	5.5	1.1	48.9	11.7	2.2	20.8	70	2.1	1.4
	1	2.6	1.1	6.8	5.5	2	48.8	9.7	1.7	21.6	75	2.2	1.2
	5	1.6	1.1	6.4	3	2.2	51.2	11.6	2.1	20.6	82	2.5	0.9
	10	1.5	1.2	7.3	2.9	2.6	52.1	10	1.8	20.5	85	2.7	0.7

		elements (atom %) and binding energies (eV)									
		Nb 3d		Se 3d			O 1s	In 3d	Sn 3d	C 1s	deg of oxidn (%)
material	oxidn time (min)	203.5 Nb^{sul}	207.5 Nb^{ox}	53.5 Se^{2-}	55 Se^{0}	59 Se^{ox}	530.6	444.6	486.8	284.8	Nb^{ox}/Nb^{total}
$NbSe_2$	0	8.8	3.6	17	1.4	0	33.6	11.5	2.1	22	29
	5	1.7	7.5	3.4	2.9	5.4	54.4	10	1.8	13	81.5
	10	1.3	8.2	2.5	2.8	5.6	56.1	8.1	1.6	13.8	86

[a] The degree of oxidation in both systems and the calculated thickness of the MoS_2/MoO_3 layers are also presented.

MoS_2 film. The S 2s and 2p lines appear at 226 and 162 eV, respectively, characteristic of S^{-2}. The peaks at about 229 and 232 eV correspond to Mo^{4+} 3d $^5/_2$ and $^3/_2$ in MoS_2, respectively. The S 2s curve fitting of this spectral window reveals that only 5% of the total Mo signal originates from an oxidized species (Mo^{5+} or Mo^{6+}) and no oxidized sulfur signal is seen (see Figure 4e and Table 2). In Figure 4b−d and f−h, the evolution of oxide signals (in both Mo and S) with increasing oxygen plasma etching time is apparent.[38] The Mo 3d envelope now includes an additional doublet at about 232.5 and 235.5 eV (Figure 4b−d) corresponding to Mo^{6+} 3d $^5/_2$ and $^3/_2$, respectively.[31] The new doublet between 168 and 170 eV (Figure 4f−h) corresponds to S 2p $^3/_2$ and $^1/_2$ lines of oxidized S species such as S^{6+}.[37] Already after 0.1 min (not shown in Figure 4) the degree of oxidation is ∼70% (Table 2). This number further increases, step by step (see Table 2), up to 85% for the 10-min sample. Figure 5 shows a typical curve fitting, for Figure 4c in this case, where the oxidized S 2s signal is evaluated based on the analysis of the S 2p line.

Panels a and e of Figure 6 show the Nb 3d and Se 3d spectra of the as-prepared $NbSe_2$ sample, respectively. The Nb signal already shows a partial oxidation, 29% (see Table 2), while selenium is not oxidized. Upon increasing oxygen plasma etching time (Figure 5b−d and f−h), the Nb further oxidizes, with its relative oxidized signal reaching 86% after 10 min and 93% for the 20-min sample.

Depth profiling via angular resolved measurements and Ar ion sputtering indicates that both MoS_2 and $NbSe_2$ films do not have perfect coverage of the substrate. A simplified model structure is used to quantitatively characterize the films, assuming a partial coverage, *a*, at a uniform thickness, *D*. A straightforward procedure, based on the angular dependence of photoelectron attenuation, allows a rough estimate of the surface coverage parameter, *a*, and the average film thickness (across the covered regions), *D*. Using the lines presented in Table 2, this model yields a consistent value $a \sim 0.7$ for all MoS_2 samples, with $D \sim 3.5$ nm. The induced oxidation is not found to modify these values above the experimental error. It does,

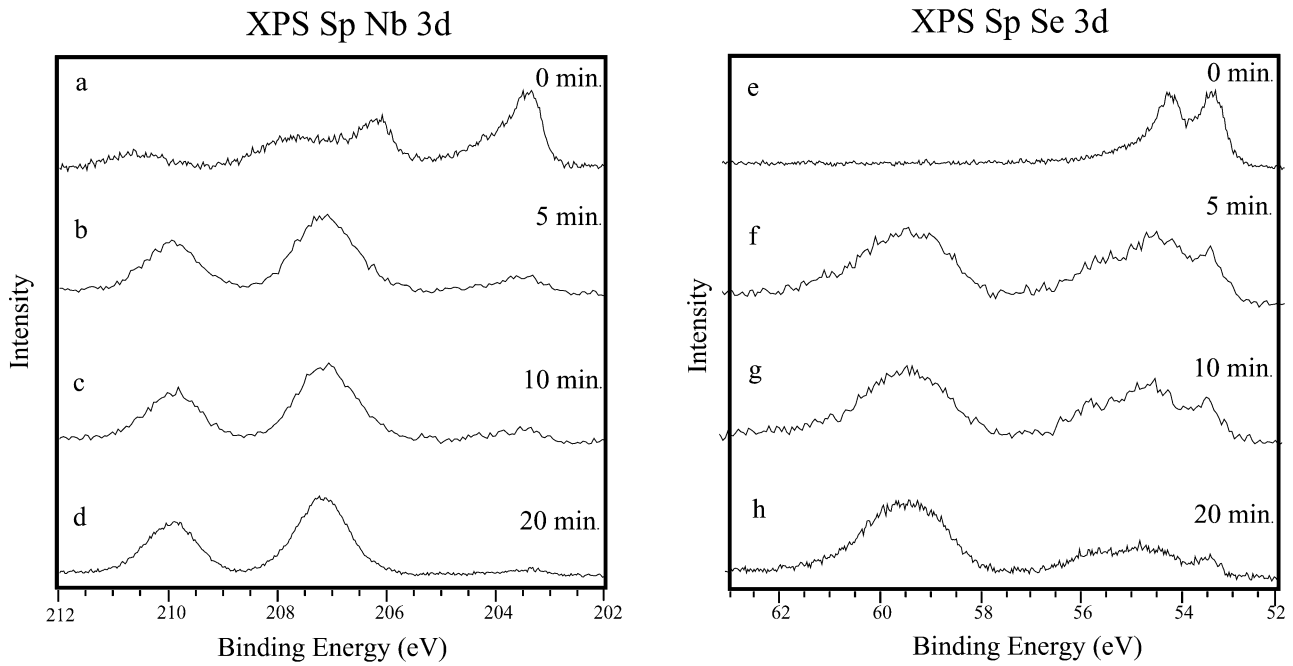

Figure 6. Nb 3d XPS spectra (a−d) and Se 2p XPS spectra (e−h) of $NbSe_2$ films after 0- (a, e), 5- (b, f), 10- (c, g), and 20-min (d, h) oxidation.

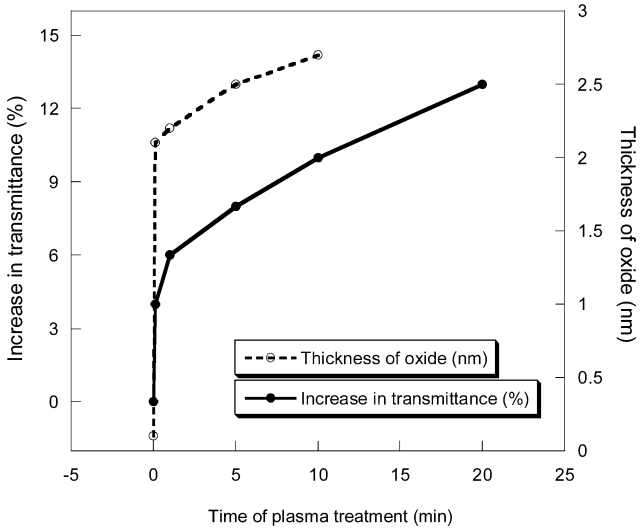

Figure 7. Thickness of the MoO_3 layer and the increase in transmittance as a function of oxidation time.

however, change the internal relative thicknesses. Supported by the AFM images, we relate the partial coverage to macroscopic imperfections such as voids between adjacent platelets in the mosaic structure. Hence, the model used to estimate the specific thicknesses of the oxide (D_1) and dichalcogenide (D_2) layers assumes a mosaic-like film structure with laterally large but very thin grains. The estimated values of D_1 and D_2 are listed in Table 2.

In the case of MoS_2, the XPS depth profile study supports the formation of a MoS_2/MoO_3 bilayer where the thickness of the oxide layer corresponds directly to the plasma oxidation time. It is also important to note that the thickness of the total inorganic film ($MoS_2 + MoO_3$) is roughly constant, indicating that the reduction in absorption is due to the conversion of MoS_2 into MoO_3 and not to evaporation of material. In Figure 7, the thickness of the MoO_3 layer and the increase in transmittance as a function of oxidation time are plotted. The XPS and transmittance results are in good agreement, showing that the rate of oxidation is not constant throughout the process. Starting with ∼3.5-nm-thick MoS_2 film (∼6 molecular layers), the upper 3 layers are oxidized in the first few seconds of oxidation. Once the upper surface is oxidized, the oxidation rate of the inner MoS_2 layers decreases and the remaining layers are gradually converted into the corresponding oxide on a time scale of minutes. This decrease in oxidation rate is associated with the slower diffusion of species through the already oxidized material.

Applying this model to the $NbSe_2$ system, the coverage parameter is $a \sim 0.6$, while the average thickness is $D \sim 5$ nm. As shown by AFM (Figure 3), the $NbSe_2$ grains in the as-deposited film are much larger than those in the as-deposited MoS_2 film and the $NbSe_2$ film is thicker. Arranging the large $NbSe_2$ platelets probably results in large voids between plates, which generate the lower coverage parameter. Furthermore, $NbSe_2$ films rapidly oxidize in ambient conditions in air as evident from the high degree of oxidation in the as-prepared film (30%). The areas of exposed substrate together with the relatively high degree of oxidation of the as-prepared $NbSe_2$ film prevent a quantitative thickness analysis of $NbSe_2/Nb_2O_5$ system using the suggested model.

PLED Device Characteristics. The LTMDC films adhere to the ITO substrate, and no delamination is observed even after long periods of time (months). They are insoluble in organic solvents, and hence, a polymer film can be spun on their surface. However, the low surface energy results in noticeably poor wetting of the LTMDC surface by the polymer solution. This local de-wetting could introduce pinholes in the polymer film upon spin-coating. The surface energy of the inorganic film is improved by oxidizing the upper layer of the LTMDC film to form the corresponding high surface energy metal oxide. Consequently, the wetting properties of the polymer solution improve remarkably.

The polymer film in the LEDs contains a 3:1 blend of an emitting polyfluorene polymer, poly(2,7-(9,9′-di-*n*-octylfluo-

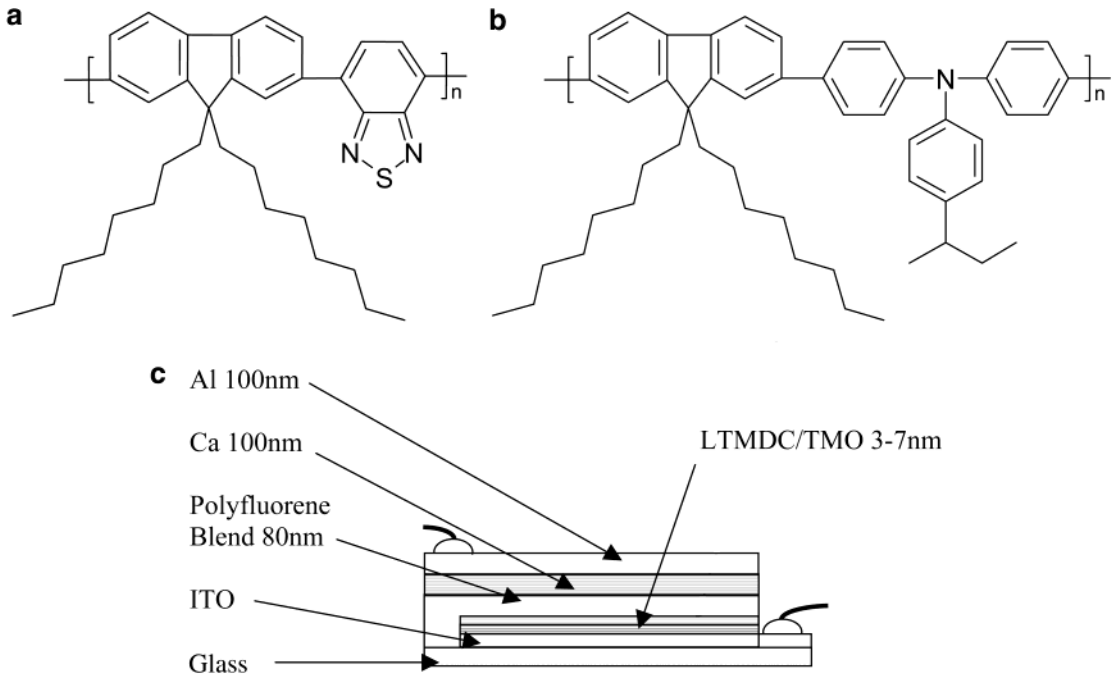

Figure 8. Schematic diagrams of the polymers and device structures: (a) poly(2,7-(9,9′-di-*n*-octylfluorene)-3,6-benzothiadiazole) (F8BT); (b) poly-(2,7(9,9-di-*n*-octylfluorene)−(1,4-phenylene-((4-*sec*-buthylphenyl)imino)-1,4-phenylene)) (TFB); (c) LED structure.

rene)-3,6-benzothiadiazole) (F8BT), and a polyfluorene hole-transporting polymer, poly-(2,7(9,9-di-*n*-octylfluorene)−(1,4-phenylene-((4-*sec*-buthylphenyl)imino)-1,4-phenylene)) (TFB). The polymer structures are shown in Figure 8a and b, and the device structure is shown in Figure 8c. The current density−voltage (JV) and luminance−voltage (LV) characteristics of PLEDs utilizing the MoS_2/MoO_3 and $NbSe_2/Nb_2O_5$ films are presented in Figures 9 and 10, respectively.

The most noticeable feature in Figure 9A is the fact that the leakage current (the current density when the device is "off" (applied bias <2 V) steadily decreases as the time of oxidation increases. For example, the leakage current in the device comprising a 20-min etched film is 2 orders of magnitude lower than that in the device using an as-prepared MoS_2 film at −6 V. The high leakage currents in the as-prepared MoS_2 films are associated with the local de-wetting of the polymer from the as-prepared LTMDC. The polymer wetting improves when the surface is oxidized. As the thickness of the oxide layer increases, the long-range interactions with the underlaying MoS_2 decreases, as observed for polymer wettability on Si surfaces with controlled coating thickness.[39] The improved wetting reduces the number of pinholes and gradually the leakage currents decrease.

In the case of $NbSe_2/Nb_2O_5$ (Figure 10A), all devices show high leakage currents regardless of the length of the oxidation treatment. This is in good agreement with the XPS and AFM data indicating lower coverage parameter, rough surfaces, and a relatively high oxidation of the as-prepared film. The polymer solution locally de-wets the surface and spun films contain pinholes regardless of the oxidation treatment.

The current densities in the "on" state of the MoS_2/MoO_3 devices are all similar (500−1000 mA/cm^2 at 6 V) with the currents slightly increasing in the sequence: 10 < 20 < 0 < 5 < 1 min of oxidation as shown in Figure 9A. The same sequence also describes the increase in luminance intensity at 6 V as a function of oxidation time (Figure 9B), except for the 0-min sample. While the devices comprising a MoS_2/MoO_3 bilayer (oxidation time >0 min) show very high luminance intensity, (2−5) × 10^4 cd/m^2, the luminance intensity in the device with an as-prepared MoS_2 film is more than 2 orders of magnitude lower. The forward ("on") currents are also similar in all $NbSe_2/Nb_2O_5$ devices ranging from 1100 mA/cm^2 in the 5- and 20-min samples to 3000 mA/cm^2 for the 10-min sample, at 6 V (Figure 10A). The luminance intensity is again similar for all devices comprising an $NbSe_2/Nb_2O_5$ bilayer ((2−5) × 10^4 cd/m^2 at 6 V) but is 2 orders of magnitude lower in the as-prepared $NbSe_2$ device (Figure 10B).

The MoS_2/MoO_3 and $NbSe_2/Nb_2O_5$ device performances in terms of power efficiencies and photometric efficiencies as function of oxidation time are tabulated in Table 3. In general, PLEDs comprising the LTMDC/TMO layers exhibit extremely high brightness (>10^4 cd/m^2) more than 2 orders of magnitude brighter than display requirement at a moderate applied bias of 6 V. Furthermore, the power efficiencies reported in this study are among the highest reported for PLEDs.[2]

We consider that the relatively low luminance in devices with untreated LTMDC is associated with exciton quenching at the metallic LTMDC film. The high electron mobility in F8BT results in locating the emission zone close to the anode. This emission is partly quenched at the mirrorlike LTMDC surface, and the total emission is decreased. By shifting the emission zone away from the electrodes, we expect the device performance to enhance. This goal is also achieved by depositing the TMO film between the LTMDC layer and the polymer. The wide-gap (3−4 eV) semiconducting TMO films act as an electron-blocking layer blocking the electrons from advancing toward the anode. Consequently, the holes injected from the anode tunnel through the oxide barrier into the electron high-

(38) The O 1s line (not shown) consists of two dominant components, associated with the substrate. These peaks mask the spectral region of the Mo (Nb) oxide. Thus, curve fitting of the O 1s does not provide a helpful input to the above analysis, which extends beyond the total oxygen intensity.
(39) Sharma, A.; Reiter, G. *J. Colloid Interface Sci.* **1996**, *178*, 383.

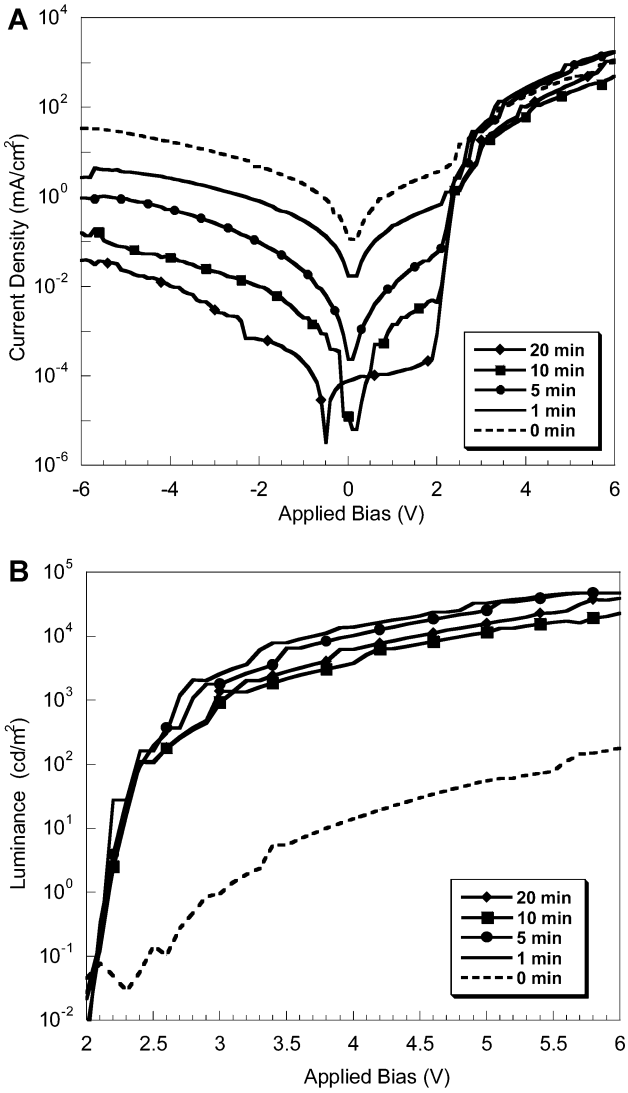

Figure 9. (A) current density−voltage and (B) luminance−voltage characteristics of PLEDs comprising the MoS_2/MoO_3 film.

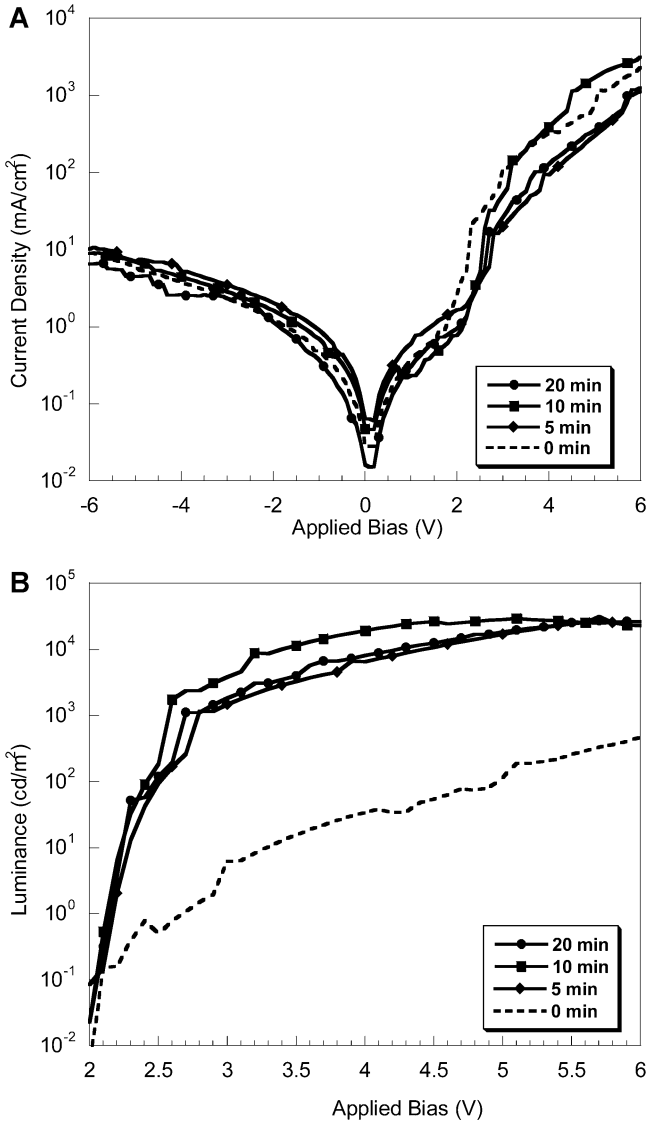

Figure 10. (A) Current density−voltage and (B) luminance−voltage characteristics of PLEDs comprising the $NbSe_2/Nb_2O_5$ films.

density region and recombine radiatively. Furthermore, the high electron density formed at the oxide/polymer interface enhances the hole injection and results in a lower light-turn-on voltage.

Therefore, the oxidation of the LTMDC improves device performance by (I) reducing the leakage currents by improving the wetting properties of the film, (II) immobilizing the electrons to form a high electron density at the TMO/polymer interface, which ensures that the holes pass within a collision capture radius of an electron, and (III) the high electron density at the TMO/polymer also increases the electric field, which improves hole injection.

As mentioned earlier, the oxidation process of MoS_2 is lateral and results in a MoO_3 continuous layer on the MoS_2. The graded improvement of the device performance with oxidation time in the MoS_2/MoO_3 system is associated with the increase of the oxide layer with oxidation time. A detailed study of the effect of the oxide thickness (barrier thickness) on the current density, luminance, and turn-on voltage in ITO/MoS_2/MoO_3/F8BT/Ca/Al devices is currently underway.[40] A profound understanding of this dependence is expected to enable the tailoring of LTMDC/TMO anodes for optimal device performance.

Table 3. Device Performances as a Function of Oxidation Time

material	oxidn time	max power effic (lm/W)	applied bias at max power effic (V)	luminance at max power effic (cd/m²)	photometric effic at max power effic (cd/A)
MoS_2	1	8.0	2.7	1380	6.8
MoS_2	5	9.1	2.6	330	7.5
MoS_2	10	10.3	2.4	100	7.8
MoS_2	20	9.7	2.4	100	7.4
$NbSe_2$	5	8.0	2.8	1160	4.3
$NbSe_2$	10	8.6	2.6	1580	9.2
$NbSe_2$	20	7.4	2.7	990	6.5

Conclusions

In this study, the use of solution-processed inorganic material in an optoelectronic device has been demonstrated by utilizing a LTMDC/TMO bilayer in PLEDs. The deposition of the LTMDC films through their intercalation and exfoliation generalized the solution processing of thin-film semiconducting

(40) Reynolds, K. J.; Barker, J. A.; Greenham, N. C.; Friend, R. H.; Frey, G. L. *J. Appl. Phys.* **2002**, *92*, 7556.

devices to include inorganic as well as organic layers. The LTMDC/TMO system demonstrates that improved device performance is achieved by controlling both hole injection, through the high work function of the LTMDC component, and electron extraction, through the blocking feature of the TMO component. The LTMDC/TMO anodes prepared in this study lead to devices with very high performances, 1000 cd/m^2 (10 times brighter than display requirements), at very low voltages (2.4−2.5 V). Finally, the range of the electronic properties of the LTMDC/TMO materials offers a unique route to optimize device performance through selection of suitable inorganic and polymeric materials in the hybrid devices.

Acknowledgment. We thank C. Ramsdale for SEM measurements, A. D. Yoffe for helpful discussions, and Cambridge Display Technology (CDT) for supply of the polymers. We acknowledge support from the Engineering and Physical Sciences Research Council and the European Commission (G.L.F., Marie-Curie Fellowship).

JA020913O